THE JOURNAL OF PHYSICAL CHEMISTRY B

Article

pubs.acs.org/JPCB

Weak Epitaxy Growth of Phthalocyanine on Inducing Layers of Fluorinated 5,5″-Bis(biphenyl-4-yl)-2,2′:5′,2″-terthiophene

Xiaolan Qiao, Lizhen Huang, Jidong Zhang, Hongkun Tian, Yanhou Geng, and Donghang Yan*

State Key Laboratory of Polymer Physics and Chemistry, Changchun Institute of Applied Chemistry, Chinese Academy of Sciences, and Graduate School of Chinese Academy of Sciences, Changchun 130022, People's Republic of China

Supporting Information

ABSTRACT: Weak epitaxy growth (WEG) is an effective method in the preparation of high-mobility thin films of disk-like organic semiconductors. The growth behavior and quality of the epitaxial thin film are closely related to the inducing layers. Here, a series of fluorinated molecules, 5,5″-bis(3′-fluoro-biphenyl-4-yl)-2,2′:5′,2″-terthiophene (*m*-F2BP3T), 5,5″-bis(3′,5′-difluoro-biphenyl-4-yl)-2,2′:5′,2″-terthiophene (F4BP3T), and 5,5″-bis(4′-fluoro-biphenyl-4-yl)-2,2′:5′,2″-terthiophene (*p*-F2BP3T) as well as a referenced molecule 5,5″-bis(biphenyl-4-yl)-2,2′:5′,2″-terthiophene (BP3T), are introduced to serve as inducing layers for the epitaxy growth of phthalocyanine. Compared to the nonfluorinated inducing layer, the interactions between the fluorinated inducing layer and phthalocyanine might be relatively strong due to the potential existence of C−H···F weak hydrogen bonds. The growth behavior and mechanism of phthalocyanine on the fluorinated inducing layers are investigated by atomic force microscopy (AFM), grazing incidence X-ray diffraction (GIXD), selected area electron diffraction (SAED). According to the AFM and SAED, H_2Pc presents a selective epitaxy growth depending on the position of fluorine: epitaxy growth on *m*-F2BP3T and F4BP4T, and nonepitaxy growth on *p*-F2BP3T. Comparison of CuPc with F_{16}CuPc on monolayer *p*-F2BP3T further revealed that the uncommon nonepitaxy growth behavior of H_2Pc (CuPc) on *p*-F2BP3T mainly originates from the enhanced interactions between the two types of molecules. As a consequence, the capability of molecules orienting themselves along the surface channel is decreased; meanwhile, the demand of the upper limit of the lattice mismatch is more rigorous for commensurate epitaxy. Finally, the oriented nucleation of H_2Pc (CuPc) on monolayer *p*-F2BP3T is affected, and netlike crystals are formed. The sudden change of H_2Pc (CuPc) from multiorientation on monolayer to just one orientation on double-layer *p*-F2BP3T suggests that there is a critical lattice mismatch value for commensurate epitaxy in WEG when the molecule−substrate interactions are enhanced.

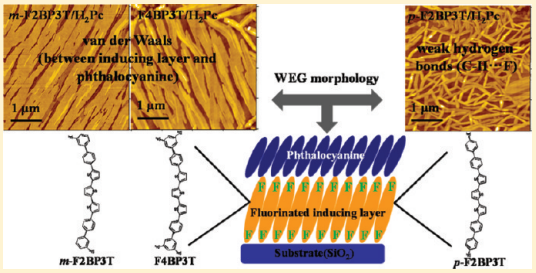

1. INTRODUCTION

In recent decades, organic semiconductor thin films have sparked enormous interest due to their crucial role in organic electronics, which possess the advantages of flexibility, low-cost, and modifying properties.[1,2] A large number of studies have shown that the orientation and quality of organic thin films are responsible for device performances.[3−7] Molecule−substrate interactions play an important role in dominating the orientation and crystallinity of the organic thin films. Traditionally, for organic molecular beam epitaxy (OMBE), organic molecules mainly grow on inorganic single-crystal substrates, and small crystals are obtained. Moreover, the organic molecules tend to lie flat on substrates due to the strong molecule−substrate electrostatic interactions.[8] By contrast, for organic vapor deposition (OVD), organic molecules grow on amorphous substrates, and polycrystalline thin films can be achieved.[9] In this method, the organic molecules tend to adopt a stand-up arrangement due to the weak molecule−substrate van der Waals interactions.[10] Other approaches such as using an oriented substrate (polytetrafluoroethylene (PTFE), pentacene, etc.) and electric field assistance are developed to adjust the orientation and to further improve the quality of organic thin films simultaneously.[11−13] Recently, a new method referred to as weak epitaxy growth (WEG) has made great progress in the preparation of high-quality organic semiconductor thin films on amorphous substrates. The mobility of transistors based on the WEG films can reach the same level as that of the corresponding single crystals.[14,15] It has been revealed that the inducing layer substrate directly determines the growth behavior and quality of the epitaxial thin film in this method.[15−18] Therefore it is necessary to expand the scope of the inducing layer to further gain insight into the mechanism of WEG.

Weak interactions, typically for weak hydrogen bonds (C−H···F, N, O), have been widely applied over the past decades because of their important role in obtaining ordered structures in supramolecular self-assembly.[19−22] Researchers have reported that F_{16}CuPc and pentacene or diindenoperylene (DIP) codeposition on metal surface can achieve two-dimensional (2D) ordered structures.[23−25] The complementary functional

Received: November 2, 2011
Revised: January 4, 2012
Published: January 11, 2012

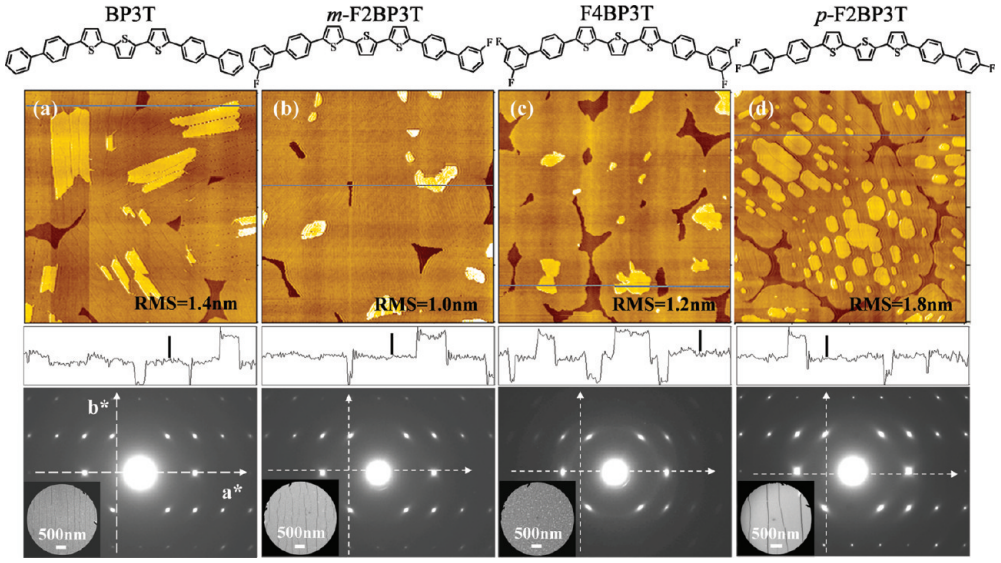

Figure 1. Molecular structures of BP3T, *m*-F2BP3T, F4BP3T, *p*-F2BP3T, and the corresponding AFM topography (20 μm × 20 μm) images of about 1 ML ultrathin films on SiO_2/Si at the substrate temperatures of 175, 175, 155, and 185 °C, as well as SAED, respectively. The height data of the films shown under each panel correspond to the blue lines indicated in the panels, and the height scale bars is 3 nm.

binary system has the potential to form C−H···F weak hydrogen bonds, which can be tuned by changing the mixture ratios, and diverse ordered binary structures can be obtained. In the WEG method, the mechanism has been studied clearly when there are only van der Waals interactions between the inducing layer (end-capped by phenyl) and phthalocyanine.[16−18] Hence, it is indispensable to clarify the mechanism of WEG when the molecule−substrate interactions are not only van der Waals but also other weak interactions.

In this paper, we purposively introduce a new series of molecules, i.e., 5,5″-bis(biphenyl-4-yl)-2,2′:5′,2″-terthiophene (BP3T) and its fluorinated derivatives 5,5″-bis(3′-fluoro-biphenyl-4-yl)-2,2′:5′,2″-terthiophene (*m*-F2BP3T), 5,5″-bis-(3′,5′-difluoro-biphenyl-4-yl)-2,2′:5′,2″-terthiophene (F4BP3T), and 5,5″-bis(4′-fluoro-biphenyl-4-yl)-2,2′:5′,2″-terthiophene (*p*-F2BP3T) (Figure 1), to act as the inducing layer in WEG. The interactions between phthalocyanine and the fluorinated inducing layer might be relatively stronger due to the potential existence of C−H···F weak hydrogen bonds compared to that between phthalocyanine and the nonfluorinated inducing layer. It is significative to gain insight into the behavior and mechanism of phthalocyanine WEG on the fluorinated inducing layer.

2. EXPERIMENTAL SECTION

2.1. Synthesis of BP3T and Its Fluorinated Derivatives.

BP3T, 2,2′:5′,2″-terthiophene, and 5,5‴-bis(tri-*n*-butylstannyl)-2,2′:5′,2″-terthiophene were synthesized according to literature procedures.[26−28] 4-Fluorobenzeneboronic acid, 3-fluorobenzeneboronic acid, and 3,5-difluorobenzeneboronic acid were purchased from Alfa Aesar. Toluene was distilled over sodium/benzophenone. *N*,*N*-Dimethyl formamide (DMF) was dried with CaH_2 and distilled under reduced pressure. ^{1}H NMR spectra were recorded on a Bruker 300 MHz spectrometer in $CDCl_3$. Chemical shift was reported to be relative to an internal tetramethylsilane (TMS) standard for measurements. Elemental analysis was carried out on a FlashEA1112 elemental analyzer.

General Procedure for the Synthesis of the Derivatives of 4-Bromo-biphenyl. A mixture of aryl boronic acid (4.78 mmol), 4-bromo-iodobenzene (5.26 mmol), $Pd(PPh_3)_4$ (0.02 mmol), Na_2CO_3 (17.9 mmol), freshly distilled toluene (28 mL), and water (10 mL) was heated to 90 °C under Ar atmosphere. After being cooled to room temperature, the precipitation was collected by filtration and washed successively with water and acetone, then dried in vacuum. The product was further purified by recrystallization from alcohol to afford a white crystal.

4-Bromo-4′-fluoro-biphenyl: yield: 90%. ^{1}H NMR (300 MHz, $CDCl_3$) δ 7.60−7.45 (m, 4H), 7.40−7.37 (m, 2H), 7.18−7.08 (m, 2H).

4-Bromo-3′-fluoro-biphenyl: yield: 90%. ^{1}H NMR (300 MHz, $CDCl_3$) δ 7.61−7.53 (m, 2H), 7.45−7.42 (m, 2H), 7.41−7.37 (m, 1H), 7.34−7.31 (m, 1H), 7.27−7.21 (m, 1H), 7.11−6.98 (m, 1H).

4-Bromo-3′,5′-difluoro-biphenyl: yield: 80%. ^{1}H NMR (300 MHz, $CDCl_3$) δ 7.85 (d, 2H), 7.41 (d, 2H), 7.11−7.02 (m, 2H), 6.84−6.77 (m, 1H).

General Procedure for the Synthesis of Derivatives of BP3T. A mixture of the derivatives of 4-bromo-biphenyl (8.00 mmol), 5,5‴-bis(tri-*n*-butylstannyl)-2,2′:5′,2″-terthiophene (3.62 mmol), $Pd(PPh_3)_4$ (0.04 mmol), and freshly distilled DMF (100 mL) was heated to 100 °C for 36 h under Ar atmosphere. After the mixture was cooled to room temperature, the precipitation was collected by filtration and washed successively with water and acetone. The product was further purified by vacuum sublimation twice before characterization to afford an orange crystal.

5,5″-Bis(4′-fluoro-biphenyl-4-yl)-2,2′:5′,2″-terthiophene (*p*-F2BP3T): yield: 70%. Anal. Calcd for $C_{36}H_{22}F_2S_3$: C, 73.44; H, 3.77; Found: C, 73.20; H, 3.92.

5,5″-Bis(3′-fluoro-biphenyl-4-yl)-2,2′:5′,2″-terthiophene (*m*-F2BP3T): yield: 66%. Anal. Calcd for $C_{36}H_{22}F_2S_3$: C, 73.44; H, 3.77; Found: C, 73.34; H, 3.98.

5,5″-Bis(3′,5′-difluoro-biphenyl-4-yl)-2,2′:5′,2″-terthiophene (F4BP3T): yield: 72%. Anal. Calcd for $C_{36}H_{20}F_4S_3$: C, 69.21; H, 3.23; Found: C, 69.02; H, 3.42.

dx.doi.org/10.1021/jp210535q | *J. Phys. Chem. B* 2012, 116, 1812−1818

2.2. Fabrication of Organic Thin Films. The MPc's were purchased from Aldrich Co. All the materials were purified twice by thermal gradient sublimation prior to experiments. A heavily doped n-type silicon wafer with a 300 nm thermal oxidation SiO_2 layer was used as the substrate. First, 3 nm BP3T series thin films with different substrate temperatures were deposited on SiO_2 substrate with a typical grain size of 60−100 μm^2. Then, MPc thin films were deposited on the series BP3T thin films. The substrate temperatures for growth of H_2Pc on BP3Ts are all 125 °C, and it is 160 °C for growth of CuPc and $F_{16}CuPc$. The deposition of all the thin films is performed under a pressure of 10^{-4} to 10^{-5} Pa at a rate of about 1 nm/min.

2.3. Atomic Force Microscopy (AFM) Measurements. Film morphologies were imaged by a SPI 3800/SPA 300HV (Seiko Instruments Inc., Japan) with tapping mode. A 150 μm scanner and a commercially available SiN4-cantilever with a spring constant of 3 N/m were used in all experiments.

2.4. X-ray Diffraction (XRD) Measurements. GIXD measurements were carried out at Shanghai Synchrotron Radiation Facility (SSRF) on beamline BL14B1 with λ = 1.24 Å. An incidence angle of 0.16° was chosen to optimize the signal-to-background ratio. The 2D image diffraction patterns were recorded using a MAR3450 detector.

2.5. Transmission Electron Microscopy (TEM) Measurements. Organic films were deposited on the SiO_2/Si substrate first; subsequently, a carbon thin film used as a support layer was deposited on the films. The films were separated from the SiO_2 surface by floating from 10% HF solution and then were transferred to a copper grid for measurements. Au was directly deposited on the samples for demarcating if necessary. The selected area electron diffraction (SAED) was performed by a JEOL JEM-1011 transmission electron microscope operated at 100 kV. Dark field was used for experiments to provide weaker-intensity beam and high contrast.

3. RESULTS AND DISCUSSION

3.1. Morphologies and Structures of Monolayer BP3T and Its Fluorinated Derivatives. As the inducing layer in the WEG method, the morphologies of BP3T and its fluorinated derivatives are crucial for the subsequent epitaxy growth. Furthermore, suitable molecule arrangement is desired for heteroepitaxy of phthalocyanine. Hence, we investigated the film morphologies and structures of the fluorinated molecules first.

The morphologies and corresponding SAED patterns of BP3T, *m*-F2BP3T, F4BP3T, and *p*-F2BP3T are given in Figure 1. The growth temperature of the thin films, optimized through experiment like *p*-6P,[29] is between 160 and 180 °C due to their different thermal properties. The coverage of all the thin films is about 1 ML. Coalescence between compact islands can be observed clearly. The average single domain size is 5−10 μm, and root-mean-square (rms) roughness is in the range of 1−2 nm. The results imply that all the thin films with large grain size are smooth enough for WEG substrates. According to the height profiles of the films, the layers' heights are all about 3 nm, comparable to the long axis of the four types of molecules. This indicates that the molecules are nearly upright on SiO_2 substrate with the long molecular axis normal to the substrate surface. The corresponding SAED of BP3T monolayer films shows a uniform 2D lattice pattern (rectangle lattice), and the strong diffraction spots indicate that all the films are highly crystalline. Moreover, the position and number of the fluorine-dependent film growth behavior has been also observed. For BP3T, *m*-F2BP3T, and F4BP3T, the density of the nucleus of the second layer approaches that of the first layer. For *p*-F2BP3T, the density of the nucleus of the second layer is much larger than that of the first layer (Supporting Information S1), and the molecules can nucleate at every site of the first layer. This suggests that the diffusion length of *p*-F2BP3T on the first layer is shorter than the molecules on the SiO_2 surface.

Figure 2 shows the 2D-GIXD pattern of 20 nm-thick BP3Ts films deposited on SiO_2. Rod-like diffraction spots in the

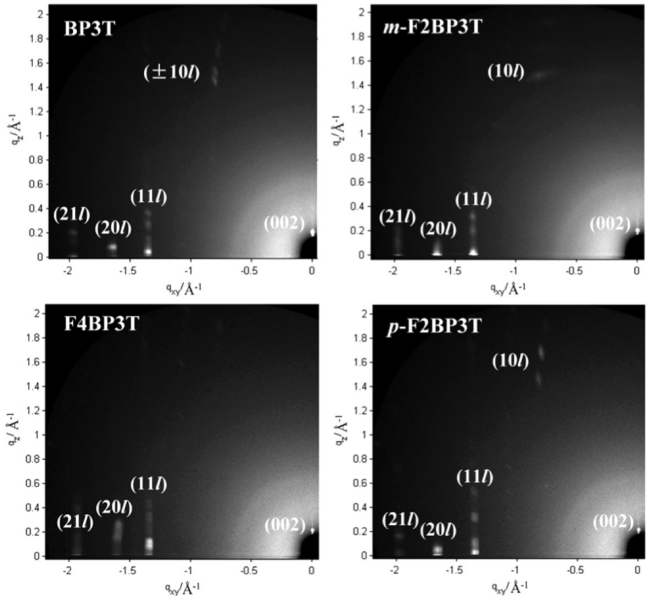

Figure 2. 2D GIXD patterns of 20 nm-thick BP3Ts films on SiO_2/Si substrates.

direction of q_z (out-of-plane) at a given q_{xy} (in-plane) strongly suggest that the *ab*-planes of BP3Ts crystallites are parallel to the interface with good registry between layers (along the *c* direction). The diffraction spots were indexed, and details of the unit cell parameters are listed in Table 1. Thin film

Table 1. Unit Cell Parameters of BP3T and Its Derivatives Extracted from the Corresponding 2D GIXD

	a/Å	*b*/Å	*c*/Å	α	β	γ
BP3T	7.53	5.78	60.00	90°	92.81°	90°
m-F2BP3T	7.66	5.85	61.04	90°	90°	90°
F4BP3T	7.76	5.87	60.65	90°	90°	90°
p-F2BP3T	7.50	5.89	62.31	98.4°	90°	90°

structure of BP3T is almost the same as that of its single crystals.[30] Moreover, the absence of (01*l*) and presence of (21*l*) peaks usually indicate a herringbone packing motif,[31] agreeing well with the SAED of monolayer BP3Ts. The accurate in-plane structures of monolayer BP3Ts and bilayer *p*-F2BP3T were further tested (Figure 3), since the direct contact of the first layer to the SiO_2 substrate and size effect may result in new structure for the first few layers.[16,17,32] The diffraction patterns of all the BP3T films show three diffraction peaks that correspond to (11*l*), (20*l*), and (21*l*). The calculated *d* spacing is given in Table 2, which provides essential data for the subsequent calculation of lattice mismatch.

dx.doi.org/10.1021/jp210535q | J. Phys. Chem. B 2012, 116, 1812−1818

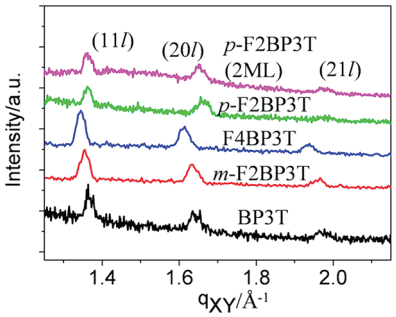

Figure 3. In-plane GIXD scans of monolayer BP3T, *m*-F2BP3T, F4BP3T, *p*-F2BP3T, and double-layer *p*-F2BP3T films. Peaks of the respective films possess the same indices, but there is little difference in q_{xy}.

3.2. Morphologies of Phthalocyanine Grown on Fluorinated Inducing Layers. On the basis of above-discussed results, the introduction of fluorine atoms in BP3T brings a distinct difference in thin film growth behavior and small change in *d* spacing, but all the molecules can form large domains with smooth surface and stand up on the SiO_2 substrate with the long molecular axis normal to the substrate surface nearly. In addition, all the molecules maintain herringbone packing motif. All of these make them suitable to act as the inducing layer in WEG. Then, we investigate the morphologies of phthalocyanine grown on the fluorinated inducing layers.

Figure 4 shows the AFM morphologies of 3 nm H_2Pc deposited on monolayer BP3Ts and the corresponding SAED patterns. Morphologies of H_2Pc crystals exhibit extraordinary differences as variation of the number and position of fluorine. On BP3T, *m*-F2BP3T, and F4BP3T, H_2Pc are stripe-like crystals with large size and possess properties of liquid-crystal, i.e., wetting the substrate. However, on *p*-F2BP3T, H_2Pc are netlike crystals with small size and possess properties of crystal, i.e., dewetting the substrate. When the substrate temperature for growth of H_2Pc is increased to 150 °C, even to 185 °C, H_2Pc still exhibited crystal-like characteristic (Supporting Information S2). The results indicate that the glass transition temperature (T_g) is prominently higher for H_2Pc grown on *p*-F2BP3T, so the ultrathin film could not exhibit liquid-crystal-like behavior at these temperatures.[33−35] The results reveal that the interactions between H_2Pc and *p*-F2BP3T are strong. The epitaxial relationship between H_2Pc and BP3Ts were investigated by SAED. Similar to H_2Pc grown on *p*-6P, diffraction spots of the (002), (01*l*) planes of H_2Pc and the (200), (020) planes of BP3Ts appear, which indicates that the (200) plane of H_2Pc is in contact with the (002) plane of BP3Ts substrates. However, the orientation is different. H_2Pc crystals show two symmetrical orientations in each domain of BP3T corresponding to incommensurate epitaxy. The angle of c^*_{H2Pc} with respect to a^*_{BP3T} is about ±13 °. H_2Pc crystals show three orientations in each domain of *m*-F2BP3T and F4BP3T corresponding to incommensurate epitaxy and commensurate epitaxy. For incommensurate epitaxy, the angle between c^*_{H2Pc} and $a^*_{m\text{-}F2BP3T}$, a^*_{F4BP3T} are about ±10° and ±13°, respectively. For commensurate epitaxy, the relationship between H_2Pc and each molecule is as follows: $(100)_{H2Pc}//(001)_{BP3Ts}$, $[001]_{H2Pc}//[100]_{BP3Ts}$, $[010]_{H2Pc}//[010]_{BP3Ts}$. However, on *p*-F2BP3T, the

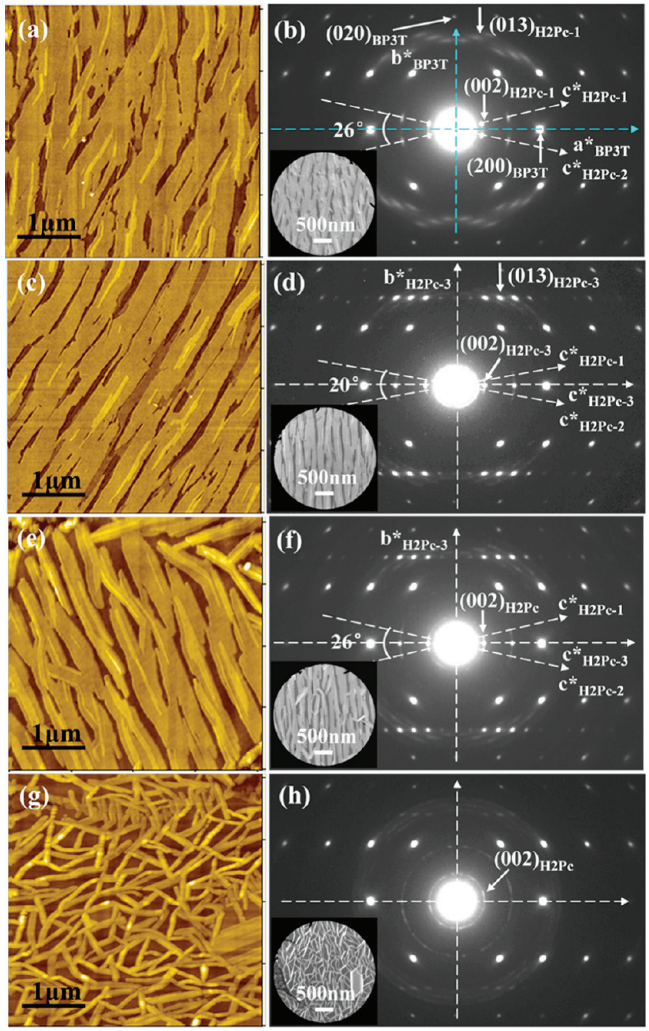

Figure 4. AFM topography of 3 nm H_2Pc grown on monolayer BP3T (a), *m*-F2BP3T (c), F4BP3T (e), and *p*-F2BP3T (g) and the corresponding SAED patterns.

Table 2. Calculated *d* Spacing from the Corresponding In-Plane GIXD and Mismatches and Oriented Angles between H_2Pc and BP3Ts (mismatch % = $(a_{inducinglayer} - a_{H2Pc})/a_{H2Pc}$)[a]

				commensurate epitaxy		incommensurate epitaxy
	d(200)/Å	*d*(010)/Å	*d*(110)/Å	$b_{inducinglayer}$ & b_{H2Pc} mismatch/%	$a_{inducinglayer}$ & c_{H2Pc} mismatch/%	$a^*_{inducinglayer}$ & c^*_{H2Pc} θ/(°)
BP3T	3.82	5.76	4.60	0.68	−4.36	13
m-F2BP3T	3.85	5.83	4.65	1.90	−3.61	10
F4BP3T	3.90	5.85	4.68	2.25	−2.36	13
p-F2BP3T	3.77	5.83	4.61	1.90	−5.61	
p-F2BP3T (2 ML)	3.80	5.78	4.60	1.03	−4.86	

[a]Lattice parameters of H_2Pc: a = 26.14 Å, b = 3.814 Å, c = 23.97 Å, α = 90°, β = 91.1°, γ = 90°.

dx.doi.org/10.1021/jp210535q | J. Phys. Chem. B 2012, 116, 1812−1818

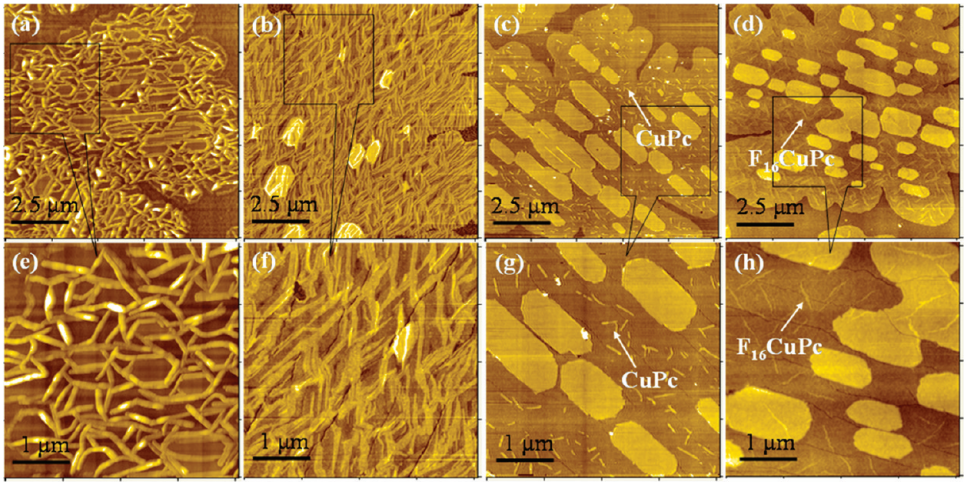

Figure 5. AFM topography of CuPc and F_{16}CuPc grown on monolayer *p*-F2BP3T: (a) CuPc (3 nm)/*p*-F2BP3T; (b) F_{16}CuPc (3 nm)/*p*-F2BP3T; (c) CuPc (0.2 nm)/*p*-F2BP3T, and (d) F_{16}CuPc (0.2 nm)/*p*-F2BP3T; (e–h) corresponding zoom images of a–d, respectively.

(002) diffraction of H_2Pc is arc, which indicates that the H_2Pc film is polycrystalline with multiorientations coincident with the AFM morphology. However, the orientation corresponding to commensurate epitaxy also exists. The lattice mismatch and the angles of a^*_{BP3Ts} and c^*_{H2Pc} are summarized in Table 2. The mismatch is in the range of 0–6%, which is much less than the upper limit (10–15%) of epitaxy growth for organic molecules.[36] The results indicate that H_2Pc presents selective epitaxy growth depending on the position of fluorine.

Channel effect and lattice match dominate the nucleation and subsequent growth of phthalocyanine in WEG. It is unambiguous that BP3T as well as its derivatives stand up on the SiO_2 substrate and possess herringbone packing mode, which provide the same configuration of surface channel. Hence, containing F atoms on the surface for *p*-F2BP3T, *m*-F2BP3T, and F4BP3T is the only difference from BP3T, which only contains H atoms. Researchers have reported that C–H can form weak hydrogen bonds with F.[37,38] Thereby, the potential formation of C–H···F weak hydrogen bonds provided by H_2Pc and the fluorinated inducing layer, respectively, may affect the oriented growth of H_2Pc. The highest points of the *m*-F2BP3T and F4BP4T surface are still H atoms in contrast to the F atoms of the *p*-F2BP3T surface. Thus there are only van der Waals (CH···H) and almost no C–H···F bonds owing to the longer distance between H_2Pc and the F atoms of *m*-F2BP3T or F4BP4T. However, there might be C–H···F bonds between H_2Pc and the prominent F atoms of *p*-F2BP3T, leading to the enhancing of the interactions between them. Accordingly, the morphology of H_2Pc growth on *p*-F2BP3T is a special one.

To further understand the effect of relatively strong molecule–substrate interactions on the morphology of phthalocyanine, we compared the growth behavior of CuPc with F_{16}CuPc on monolayer *p*-F2BP3T. There might also be C–H···F weak hydrogen bonds between CuPc and *p*-F2BP3T. However, the periphery of F_{16}CuPc is F atoms, so the interactions between F_{16}CuPc and *p*-F2BP3T (CF···F) are considered to be van der Waals, which are same as the interactions between H_2Pc and BP3T (CH···H). The morphologies of 3 and 0.2 nm CuPc and F_{16}CuPc on *p*-F2BP3T are shown in Figure 5. It is netlike crystals for 3 nm CuPc, similar to H_2Pc (Figure 5a and e). By contrast, it is oriented texture for F_{16}CuPc (Figure 5b and f). Obviously, the enhanced interactions play an important role in tailoring the morphology of CuPc. Figure 5c,g,d,h shows 0.2 nm CuPc and F_{16}CuPc on *p*-F2BP3T, and it is clear that randomly oriented nuclei have been formed at the initial stage for CuPc. However, there are just two types of oriented nuclei for F_{16}CuPc. In addition, the nucleus's density of CuPc is much larger than that of F_{16}CuPc, implying that the diffusion length of CuPc is relatively shorter. The results suggest that the interactions between CuPc and *p*-F2BP3T are indeed stronger than that between F_{16}CuPc and *p*-F2BP3T, and the enhanced molecule–substrate interactions work on the thin film morphology from the nucleation stage.

3.3. Mechanism of WEG for Phthalocyanine Grown on *p*-F2BP3T. According to our previous work, phthalocyanine molecules will diffuse along the surface channel, which is formed by the prominent H atoms for phenyl ended-capped molecules such as *p*-6P and so forth, and consequently form oriented nuclei by colliding with the other molecules. However, when the surface channel is formed by prominent F atoms, such as *p*-F2BP3T, the growth of H_2Pc or CuPc brings the potential to fashion C–H···F weak hydrogen bonds. Theoretically speaking, the relatively strong molecule–substrate interactions will decrease the capability of the molecules orienting themselves along the surface channel and facilitate the registry of overlayer lattice to the inducing layer lattice. That is, lattice match will exhibit a prominent effect for this situation, therefore realizing the unique orientation corresponding to commensurate epitaxy. Actually, things go contrary to our wishes: H_2Pc (CuPc) present multiorientations, although the lattice mismatch is much less than the upper limit of epitaxy growth for organic molecules. This reflects the fact that the strain is too large for *p*-F2BP3T or CuPc when they progress in lattice match. As a consequence, the nucleus dominated by lattice match will not exist steadily, either being licked up by other types nuclei or not being able to grow up. As we know, strain is originated from lattice mismatch. The larger the mismatch, the larger strain is. Thereby, the relatively strong interactions might result in a more rigorous demand of the upper limit of the lattice mismatch for WEG, beyond which the growth process will be not controlled by the lattice match effect.

Figure 6 gives the TEM dark field morphology and corresponding SAED pattern for 3 nm CuPc grown on

dx.doi.org/10.1021/jp210535q | *J. Phys. Chem. B* 2012, 116, 1812–1818

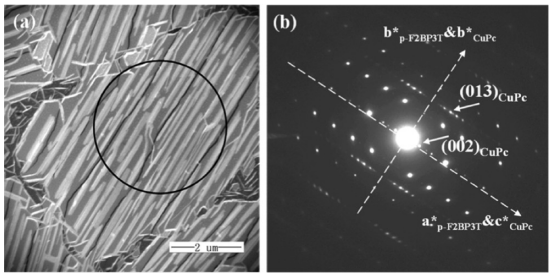

Figure 6. (a) TEM dark field morphology and (b) corresponding SAED pattern for 3 nm CuPc grown on double-layer *p*-F2BP3T.

double-layer *p*-F2BP3T. Fiber-like crystals are observed (Figure 6a). According to SAED results (Figure 6b), CuPc shows just one orientation, and it is commensurate epitaxy evidenced by the coincidence of $(006)_{CuPc}$ and $(200)_{p\text{-F2BP3T}}$, similar to H_2Pc (Supporting Information S3). It is amazing that multi-orientation on monolayer abruptly transforms to just one orientation on double-layer *p*-F2BP3T. The arrangement of the two type molecules is uniform for commensurate epitaxy (Figure 7), so the interactions between CuPc and monolayer *p*-

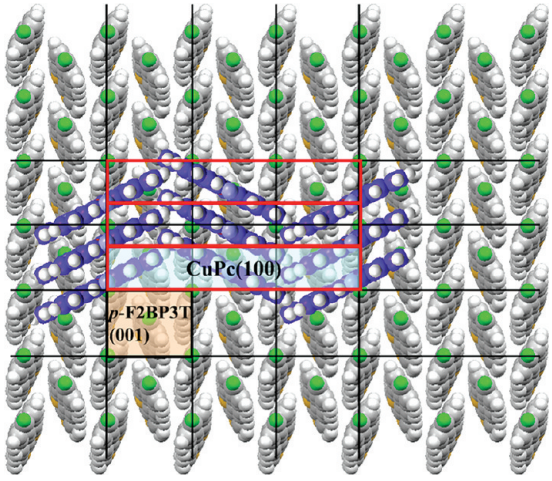

Figure 7. Schematic diagram of CuPc grown on monolayer and double-layer *p*-F2BP3T for the condition of commensurate epitaxy (top view). Red (filled by light blue) and black (filled by light orange) rectangles denote the in-plane 2D lattice of CuPc and *p*-F2BP3T, respectively.

F2BP3T is the same to that between CuPc and double-layer *p*-F2BP3T. However, the lattice parameters of monolayer and double-layer are different (Table 2), and so lattice mismatch will be different between CuPc and *p*-F2BP3T. The mismatch between CuPc and double-layer *p*-F2BP3T is shown as follows: along the [100] direction of *p*-F2BP3T, mismatch % = $(3d_{(200)p\text{-F2BP3T}} - d_{(002)CuPc})/d_{(002)CuPc} = -4.68\%$; along the [010] direction of *p*-F2BP3T, mismatch % = $(2d_{(010)p\text{-F2BP3T}} - 3d_{(010)CuPc})/3d_{(010)CuPc} = 1.67\%$. The mismatches between CuPc and monolayer *p*-F2BP3T are −5.43% and 2.55% along the [100] and [010] directions respectively. Obviously, the mismatch is smaller for CuPc and double-layer *p*-F2BP3T. The in-plane structure of *p*-F2BP3T (monolayer)/CuPc (3 nm) and *p*-F2BP3T (double-layer)/CuPc (3 nm) thin films were further tested by GIXD (Figure 8) and details of *d* spacing were given in Table 3. Moreover, the strains of *p*-F2BP3T and CuPc were shown in Table 4. The strain of double-layer *p*-F2BP3T (0.26%

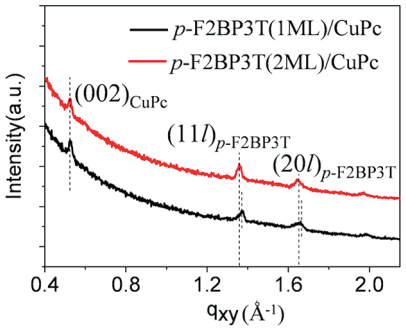

Figure 8. The in-plane structure of *p*-F2BP3T (monolayer)/CuPc (3 nm) and *p*-F2BP3T (double-layer)/CuPc (3 nm) thin films tested by GIXD.

Table 3. Details of *d* Spacing for Each Film Extracted from the Corresponding GIXD

	$d(200)_{p\text{-F2BP3T}}$	$d(010)_{p\text{-F2BP3T}}$	$d(002)_{CuPc}$
p-F2BP3T(monolayer)/CuPc	3.80	5.74	11.94
p-F2BP3T(double-layer)/CuPc	3.81	5.83	11.94

Table 4. Strains for Monolayer and Double-Layer *p*-F2BP3T and CuPc

	$\delta d(200)_{p\text{-F2BP3T}}$	$\delta d(010)_{p\text{-F2BP3T}}$	$\delta d(002)_{CuPc}$
p-F2BP3T(monolayer)/CuPc	0.79%	1.54%	0.17%
p-F2BP3T(double-layer)/CuPc	0.26%	0.86%	0.17%

and 0.86%) is indeed smaller than that of monolayer (0.79% and 1.54%), and so it is propitious to the commensurate epitaxy for CuPc growth on double-layer *p*-F2BP3T.

Taking a comprehensive view of the above-discussed, when the molecule−substrate interactions are enhanced, there will be a critical value of lattice mismatch or strain for commensurate epitaxy in WEG. Once the lattice mismatch is beyond the critical value, lattice match effect will no longer dominate the growth of phthalocyanine molecules, and multiorientations appear, i.e., H_2Pc (CuPc) growth on monolayer *p*-F2BP3T. Otherwise, there will be unique orientation corresponding to commensurate epitaxy, i.e., H_2Pc (CuPc) growth on double-layer *p*-F2BP3T. In the CuPc/*p*-F2BP3T system, the critical value is between −4.68% and −5.43%, maybe 5%. In the H_2Pc/*p*-F2BP3T system, the critical value is between −4.86% and −5.61% as shown in Table 2, also maybe 5%. The argument of critical lattice mismatch value is prevalent to explain the mechanism of WEG for planar-phthalocyanine.

4. CONCLUSIONS

Fluorinated inducing layers *m*-F2BP3T, F4BP3T, *p*-F2BP3T, and planar-phthalocyanine are introduced to further investigate the mechanism of WEG. According to AFM and SAED, H_2Pc presents a selective epitaxy growth depending on the position of fluorine. H_2Pc presents three orientations on *m*-F2BP3T and F4BP3T. However, H_2Pc presents random orientation on *p*-F2BP3T. By comparing CuPc with F_{16}CuPc growth on *p*-F2BP3T, we revealed that the molecule−substrate interactions between CuPc and *p*-F2BP3T are relatively stronger than that between F_{16}CuPc and *p*-F2BP3T. It might be due to the potential existence of C−H···F weak hydrogen bonds between CuPc and *p*-F2BP3T. The enhanced molecule−substrate

dx.doi.org/10.1021/jp210535q | J. Phys. Chem. B 2012, 116, 1812−1818

interactions decreased the capability of the molecules to orient themselves along the surface channel; meanwhile, the demand of the upper limit of the lattice mismatch is more rigorous for commensurate epitaxy in WEG. Thereby, diverse oriented nuclei followed by netlike crystals are formed. What's more, there is a critical lattice mismatch or strain for the commensurate epitaxy when the molecule−substrate interactions are enhanced. Therefore there is a sudden change of H_2Pc (CuPc) from multiorientation on monolayer to just one orientation on double-layer *p*-F2BP3T. These results will help to further understand the mechanism of WEG. In addition, the selective WEG of phthalocyanine provides a direction for synthesizing materials of inducing layers appropriately, for instance, according to position and number of the functional group.

■ ASSOCIATED CONTENT

Supporting Information

Morphologies of the initial growth of *p*-F2BP3T, H_2Pc grown on *p*-F2BP3T at different substrate temperatures, and H2Pc grown on double-layer p-F2BP3T. This material is available free of charge via the Internet at http://pubs.acs.org.

■ AUTHOR INFORMATION

Corresponding Author

*E-mail: yandh@ciac.jl.cn. Fax: +86-431-85262266. Tel: +86-431-85262165.

■ ACKNOWLEDGMENTS

This work was financially supported by the National Natural Science Foundation of China (51133007) and The National Basic Research Program (2009CB939702). The authors thank beamline BL14B1 (Shanghai Synchrotron Radiation Facility) for providing the beam time.

■ REFERENCES

(1) Forrest, S. R. *Nature* **2004**, *428*, 911.
(2) Dimitrakopoulos, C. D.; Malenfant, P. R. L. *Adv. Mater.* **2002**, *14*, 99.
(3) Bao, Z.; Lovinger, A. J.; Dodabalapur, A. *Appl. Phys. Lett.* **1996**, *69*, 3066.
(4) Bao, Z. N.; Lovinger, A. J.; Dodabalapur, A. *Adv. Mater.* **1997**, *9*, 42.
(5) Dimitrakopoulos, C. D.; Brown, A. R.; Pomp, A. *J. Appl. Phys.* **1996**, *80*, 2501.
(6) Song, D.; Wang, H.; Zhu, F.; Yang, J.; Tian, H.; Geng, Y.; Yan, D. *Adv. Mater.* **2008**, *20*, 2142.
(7) Schmidt, R.; Oh, J. H.; Sun, Y.-S.; Deppisch, M.; Krause, A.-M.; Radacki, K.; Braunschweig, H.; Koenemann, M.; Erk, P.; Bao, Z.; Wuerthner, F. *J. Am. Chem. Soc.* **2009**, *131*, 6215.
(8) Forrest, S. R. *Chem. Rev.* **1997**, *97*, 1793.
(9) Yu, X. J.; Xu, J. B.; Cheung, W. Y.; Ke, N. *J. Appl. Phys.* **2007**, *102*, 103711.
(10) Yang, J.; Yan, D. *Chem. Soc. Rev.* **2009**, *38*, 2634.
(11) Wittmann, J. C.; Smith, P. *Nature* **1991**, *352*, 414.
(12) Chen, X. L.; Lovinger, A. J.; Bao, Z. N.; Sapjeta, J. *Chem. Mater.* **2001**, *13*, 1341.
(13) Schuster, B.; Basova, T. V.; Peisert, H.; Chasse, T. *ChemPhysChem* **2009**, *10*, 1874.
(14) Wang, H.; Zhu, F.; Yang, J.; Geng, Y.; Yan, D. *Adv. Mater.* **2007**, *19*, 2168.
(15) Pan, F.; Tian, H.; Qian, X.; Huang, L.; Geng, Y.; Yan, D. *Org. Electron.* **2011**, *12*, 1358.
(16) Yang, J.; Wang, T.; Wang, H.; Zhu, F.; Li, G.; Yan, D. *J. Phys. Chem. B* **2008**, *112*, 3132.
(17) Huang, L.; Liu, C.; Yu, B.; Zhang, J.; Geng, Y.; Yan, D. *J. Phys. Chem. B* **2010**, *114*, 4821.
(18) Wang, T.; Huang, L.; Yang, J.; Tian, H.; Geng, Y.; Yan, D. *J. Phys. Chem. B* **2010**, *114*, 16408.
(19) Yokoyama, T.; Yokoyama, S.; Kamikado, T.; Okuno, Y.; Mashiko, S. *Nature* **2001**, *413*, 619.
(20) Theobald, J. A.; Oxtoby, N. S.; Phillips, M. A.; Champness, N. R.; Beton, P. H. *Nature* **2003**, *424*, 1029.
(21) Pawin, G.; Wong, K. L.; Kwon, K.-Y.; Bartels, L. *Science* **2006**, *313*, 961.
(22) Bartels, L. *Nat. Chem.* **2010**, *2*, 87.
(23) Wakayama, Y.; de Oteyza, D. G.; Garcia-Lastra, J. M.; Mowbray, D. J. *ACS Nano* **2011**, *5*, 581.
(24) Huang, Y. L.; Chen, W.; Li, H.; Ma, J.; Pflaum, J.; Wee, A. T. S. *Small* **2010**, *6*, 70.
(25) Barrena, E.; de Oteyza, D. G.; Dosch, H.; Wakayama, Y. *ChemPhysChem* **2007**, *8*, 1915.
(26) Xue, G. P.; Bradshaw, J. S.; Su, N.; Krakowiak, K. E.; Savage, P. B.; Izatt, R. M. *J. Heterocycl. Chem.* **2000**, *37*, 1.
(27) Carpita, A.; Rossi, R.; Veracini, C. A. *Tetrahedron* **1985**, *41*, 1919.
(28) Miller, L. L.; Yu, Y. *J. Org. Chem.* **1995**, *60*, 6813.
(29) Yang, J.; Wang, T.; Wang, H.; Zhu, F.; Li, G.; Yan, D. *J. Phys. Chem. B* **2008**, *112*, 7821.
(30) Hotta, S.; Goto, M.; Azumi, R.; Inoue, M.; Ichikawa, M.; Taniguchi, Y. *Chem. Mater.* **2004**, *16*, 237.
(31) Yuan, Q.; Mannsfeld, S. C. B.; Tang, M. L.; Toney, M. F.; Luening, J.; Bao, Z. *J. Am. Chem. Soc.* **2008**, *130*, 3502.
(32) Fritz, S. E.; Martin, S. M.; Frisbie, C. D. *J. Am. Chem. Soc.* **2004**, *13*, 126.
(33) Jiang, Q.; Shi, H. X.; Zhao, M. *J. Chem. Phys.* **1999**, *111*, 2176.
(34) Ellison, C. J.; Torkelson, J. M. *Nat. Mater.* **2003**, *2*, 695.
(35) Lang, X. Y.; Zhang, G. H.; Lian, J. S.; Jiang, Q. *Thin Solid Films* **2006**, *497*, 333.
(36) Wittmann, J. C.; Lotz, B. *Prog. Polym. Sci.* **1990**, *15*, 909.
(37) Coates, G. W.; Dunn, A. R.; Henling, L. M.; Dougherty, D. A.; Grubbs, R. H. *Angew. Chem., Int. Ed. Engl.* **1997**, *36*, 248.
(38) Teff, D. J.; Huffman, J. C.; Caulton, K. G. *Inorg. Chem.* **1997**, *36*, 4372.